



HAL
open science

Tsunami earthquakes: Vertical pop-up expulsion at the forefront of subduction megathrust

N.D. Hananto, Frédérique Leclerc, L. Li, M. Etchebes, H. Carton, P.
Tapponnier, Y. Qin, P. Avianto, S.C. Singh, S. Wei

► To cite this version:

N.D. Hananto, Frédérique Leclerc, L. Li, M. Etchebes, H. Carton, et al.. Tsunami earthquakes: Vertical pop-up expulsion at the forefront of subduction megathrust. *Earth and Planetary Science Letters*, 2020, 538, pp.116197. 10.1016/j.epsl.2020.116197 . hal-02506274

HAL Id: hal-02506274

<https://hal.science/hal-02506274>

Submitted on 1 Jul 2020

HAL is a multi-disciplinary open access archive for the deposit and dissemination of scientific research documents, whether they are published or not. The documents may come from teaching and research institutions in France or abroad, or from public or private research centers.

L'archive ouverte pluridisciplinaire **HAL**, est destinée au dépôt et à la diffusion de documents scientifiques de niveau recherche, publiés ou non, émanant des établissements d'enseignement et de recherche français ou étrangers, des laboratoires publics ou privés.



Distributed under a Creative Commons Attribution - NonCommercial 4.0 International License



Tsunami earthquakes: Vertical pop-up expulsion at the forefront of subduction megathrust

N.D. Hananto^a, F. Leclerc^{b,*}, L. Li^{c,d}, M. Etchebes^e, H. Carton^f, P. Tapponnier^g, Y. Qin^f, P. Avianto^a, S.C. Singh^{f,h}, S. Wei^h

^a Research Center for Deep Sea, Indonesian Institute of Sciences, Jl. Syaramanual Ambon, 97233 Indonesia

^b Géoazur, Université Côte d'Azur (U. Nice, CNRS, Observatoire de la Côte d'Azur, IRD), 250 rue Albert Einstein, CS 10269-F 06905 Sophia Antipolis, France

^c Guangdong Provincial Key Laboratory of Geodynamics and Geohazards, School of Earth Sciences and Engineering, Sun Yat-Sen University, Guangzhou, 510275, China

^d Southern Marine Science and Engineering Guangdong Laboratory (Zhuhai), Zhuhai, 519082, China

^e Schlumberger Doll Research, One Hampshire Street, Cambridge (MA), 02139, United States of America

^f Equipe de Géosciences Marines, Institut de Physique du Globe de Paris (CNRS, Paris Diderot, Sorbonne Paris Cité), 1 rue Jussieu, 75238 Paris Cedex 05, France

^g Institute of Crustal Dynamics (ICD), China Earthquake Administration (CEA), No. 1, Anningzhuang Rd., Haidian District, Beijing, 100085, China

^h Earth Observatory of Singapore, Asian School of the Environment, Nanyang Technological University, N2-01A-08, 50 Nanyang Avenue, 639798, Singapore

ARTICLE INFO

Article history:

Received 22 July 2019

Received in revised form 13 February 2020

Accepted 28 February 2020

Available online 10 March 2020

Editor: J.-P. Avouac

Keywords:

Tsunami Earthquakes
seafloor uplift source
pop-up structure
accretionary wedge
Mentawai 2010 earthquake

ABSTRACT

Published slip distribution models, based on geodetic, seismological and tsunami data, of the M_w 7.8, 2010 Mentawai tsunami earthquake offshore south-central Sumatra, suggest that the large tsunami wave was generated by a narrow swath of high seafloor uplift along the accretionary wedge front, implying higher vertical throw than that consistent with slip on the shallow-dipping megathrust. Here we present high-resolution seismic reflection profiles across the 2010 rupture zone that image the youngest deformation at the accretionary wedge front. The profiles reveal conjugate, steeply-dipping, active thrust faults that branch upwards from the megathrust and bound triangular pop-ups. The seismologically determined co-seismic slip (≥ 10 m) on the 6°-dipping decollement probably caused a comparable amount of upward expulsion of these ~ 3 km-wide, flat-topped pop-ups. Co-seismic throw on the $\approx 60^\circ$ dipping thrusts that bound the pop-up plateaus maximize the uplift of the seafloor and overlying water-column, providing an additional localised tsunami source. Tsunami simulations show that such combined deformation, i.e. the broad-scale seafloor displacement caused by slip on the megathrust and the localized 8–10 m seafloor uplift across a 6–9 km-wide pop-up belt involving up to three pop-ups, is able to reproduce the 2010 tsunami amplitude measured by a DART buoy, and observed run-up heights in the Mentawai Islands. This simple mechanism, observed in analogue sandbox shortening experiments, may thus efficiently generate the oversize waves that characterize Tsunami-Earthquakes. Systematic mapping of pop-ups along accretionary wedge fronts may help identify trench segments prone to produce the special class of seismic events that spawn exceptionally large tsunamis.

© 2020 The Authors. Published by Elsevier B.V. This is an open access article under the CC BY-NC-ND license (<http://creativecommons.org/licenses/by-nc-nd/4.0/>).

1. Introduction

Along subduction zones, devastating tsunamis may be generated by both great ($M_w \geq 8$) megathrust earthquakes (e.g. 2011 Tohoku-Oki event) and much smaller “tsunami” earthquakes. The latter constitute a special class of rare earthquakes that rupture the shallow portion of the subduction interface with low rupture velocity and stress drop, and that have the defining characteristic to trigger significantly larger tsunamis than expected from their

magnitude (Kanamori, 1972; Polet and Kanamori, 2000; Lay et al., 2012). It has been proposed that they initiate from the breakup of an asperity in the “conditionally stable” zone of the megathrust (Bilek and Lay, 2002).

For both conventional megathrust and tsunami earthquakes, the vertical component of seafloor displacement due to elastic deformation of the upper plate above the slip patch on the low-angle megathrust is thought to be the basic mechanism of tsunami generation (e.g. Satake and Tanioka, 1999). However, such mechanism can be insufficient to explain tsunami sizes, especially in the case of $M_w < 8$ Tsunami earthquakes. Other proposed tsunami source mechanisms include: 1) slip on steeply-dipping splay faults within the accretionary prism (e.g. Cummins and Kaneda, 2000), that can

* Corresponding author.

E-mail address: leclerc@geoazur.unice.fr (F. Leclerc).

be more effective at generating high seafloor uplift, whether of thrust or normal-fault type, 2) uplift associated with horizontal co-seismic displacement of sloping seafloor (i.e. front of prism, Tanioka and Satake, 1996), 3) due to seaward shoving of sediments along accretionary wedge toe (called sediment effect, Tanioka and Seno, 2001) or 4) to the release of gravitational potential energy (McKenzie and Jackson, 2012), 5) enhancement of slip due to dynamic overshoot (Ide et al., 2011) or 6) to shaking-triggered submarine landslides (Tappin et al., 2014). A full understanding of the sources triggering higher-than-expected tsunami waves requires in-situ ground truth of co-seismic seafloor structural and geomorphic changes (e.g. Okal and Newman, 2001), hitherto available in only a few rare cases (Fujiwara et al., 2011; Kodaira et al., 2012).

Here, we explore the potential of tsunami sources specific to Tsunami Earthquakes by conducting a high-resolution study of the inferred surface rupture area of the M_w 7.8, 2010 Mentawai tsunami earthquake. The detailed interpretation of high-quality seismic reflection profiles acquired across the tip of the accretionary front suggests a seafloor deformation mechanism ("Pop-up extrusion"). We propose that such a simple tectonic process, capable of maximizing localized, vertical seafloor uplift at the megathrust front, may have been responsible for the exceptional wave and run-ups observed in 2010 in the Mentawai Islands, a proposition that we then test with tsunami simulations.

2. The 2010, Mentawai tsunami earthquake

The M_w 7.8, Mentawai earthquake occurred on October 25, 2010, offshore the fore-arc islands of North and South Pagai in the southern Mentawai archipelago (Indonesia, Fig. 1). As characteristic of tsunami earthquakes, this event ruptured a shallow patch of the subduction interface (Lay et al., 2011; Newman et al., 2011; Bilek et al., 2011), up-dip of the 2007, M_w 8.4 Bengkulu mainshock and M_w 7.9 Pagai-Sipora aftershock (Konca et al., 2008) that likely triggered its occurrence (Tsang et al., 2016).

The 2010 Mentawai earthquake generated a large tsunami along >100 km of coastlines that killed over 500 people. Run-ups >6 m were measured along the coastlines of the small islands west of Pagai, with a maximum value exceeding locally 16 m, and with inundation extending more than 300 m inland (Hill et al., 2012; Satake et al., 2013).

The location and slip distribution of the event were determined from seismic arrivals and waveform inversion (Lay et al., 2011; Newman et al., 2011; Bilek et al., 2011), and were further constrained by joint inversions of seismologic and geodetic data (Hill et al., 2012) as well as by tsunami observation (Yue et al., 2014, see a summary of the main slip models in Table 1, supplementary material).

Continuous GPS stations, though located several tens of km from the epicentral zone, provide critical information on the source of the 2010 earthquake. Maximum co-seismic values of horizontal displacement (22 ± 0.5 cm shortening) and vertical displacement (4 ± 1 cm of subsidence) were obtained at a site located ~50 km northeast of the epicenter (Hill et al., 2012). Assuming a megathrust dip of 7° and a layered rigidity structure, Hill et al. calculated a co-seismic slip model from the inversion of geodetic data alone. According to this model, the maximum slip would have been only 86 cm mid-way between the trench axis and the Pagai islands, and the maximum associated seafloor uplift would have been less than 15 cm, thus incapable of producing the large observed tsunami run-up heights. Instead, the tsunami data require that a significant part of the slip occurred at shallow depths and suggest patchy slip (Satake et al., 2013; Yue et al., 2014). Hill et al. (2012) calculated another co-seismic slip model by imposing an initial a priori slip of 12 ± 0.5 m over a 120 km-long zone that extends in width from the trench to the islands and leaving the inversion to adjust the

co-seismic slip distribution to meet the GPS constraints. According to that preferred model, much of the slip was concentrated at distances less than 50 km from the trench and at depths shallower than 6 km, with a maximum slip of 9.7 m, and a maximum seafloor uplift of 1.9 m (Fig. 1).

The predictions of that preferred model, however, still underestimate the measured tsunami run-up heights and the wave height at the DART 56001 buoy, located 1600 km south-eastwards in the Indian Ocean, which recorded only a centimetre-scale, open-ocean tsunami (Newman et al., 2011). Hill et al. (2012) suggested that additional uplift generated through inelastic folding of sediments at the prism toe could have played an important role. They included inelastic folding of sediments as an "ad-hoc" additional seafloor uplift source of 2.5 m, affecting a rectangular area of 43 km along-strike and 11 km downdip, and used it to initiate the tsunami modelling along with the elastic seafloor deformation generated from the preferred co-seismic slip model. As a result of such doubling of seafloor uplift, an improved fit to the DART data was obtained, but the DART signal still remained under-predicted. Although shallow coastal bathymetry, still poorly known, and/or resonance effects might have played a role in inflating run-up heights, it seems likely that the tsunami under-prediction simply reflects larger amounts of co-seismic vertical seafloor uplift near the trench.

Through joint inversion of geodetic and teleseismic data, together with iterative forward modelling of tsunami recordings from two tide gauges and two deep-water buoys (among which DART 56001), Yue et al. (2014) obtained a co-seismic slip model that confirmed that the occurrence of large slip at very shallow depths was required to account for the large tsunami. Specifically, their model co-involves two patches on a 7.5° dipping fault. The deeper patch extends for ~80-km along strike and ~30-km along dip between depths of 7–10 km and shows up to 8 m of slip. The shallower, near-trench patch extends for ~100 km along strike and 5 km along dip and shows a maximum slip of 23 m. Seafloor uplift associated with the up-dip patch is ~5 m in a ~45 km along-trench strip. Uncertainties on maximum slip values arise both from trade-off with rigidity structure, as well as from smoothing and parameterisation choices, but Yue et al. (2014) conclude that at least 15 m of slip is needed in the near-trench strip in order to promote enough uplift to generate the observed tsunami. Therefore, the calculated near-trench slip needs to be two to three times higher than the downdip slip. It is also much larger than the strain accumulated since the last great earthquake of 1833. Yue et al. (2014) suggest that either the 2010 earthquake broke a patch left un-broken in 1833, or that over-shooting occurred during up-dip propagation of the 2010 rupture.

In order to understand the mechanisms that might have contributed to foster high 2010 uplift at the prism toe, we investigate the geometry and structures of the accretionary prism within the 2010 Mentawai rupture area by analysing high-resolution seismic reflection profiles and bathymetry.

3. Marine geophysical data and methods

The Mega-Tera survey, carried out in May–June 2015 onboard the R/V *Falkor* of Schmidt Ocean Institute, involved acquisition of seismic reflection profiles across the frontal accretionary prism (Fig. 2) that provide much higher resolution and denser coverage than previously-acquired deep penetration seismic profiles (Singh et al., 2011). A G-gun cluster was used as a seismic energy source, with a total volume of 500 cubic inches and a tow depth of 3 m, producing acoustic waves with frequencies up to 200 Hz. The shot interval was 25 m. Seismic data were recorded using a 1.2 km long streamer containing 96 channels at 12.5 m group interval, towed at 4.5 m below the sea surface. A standard seismic reflection data

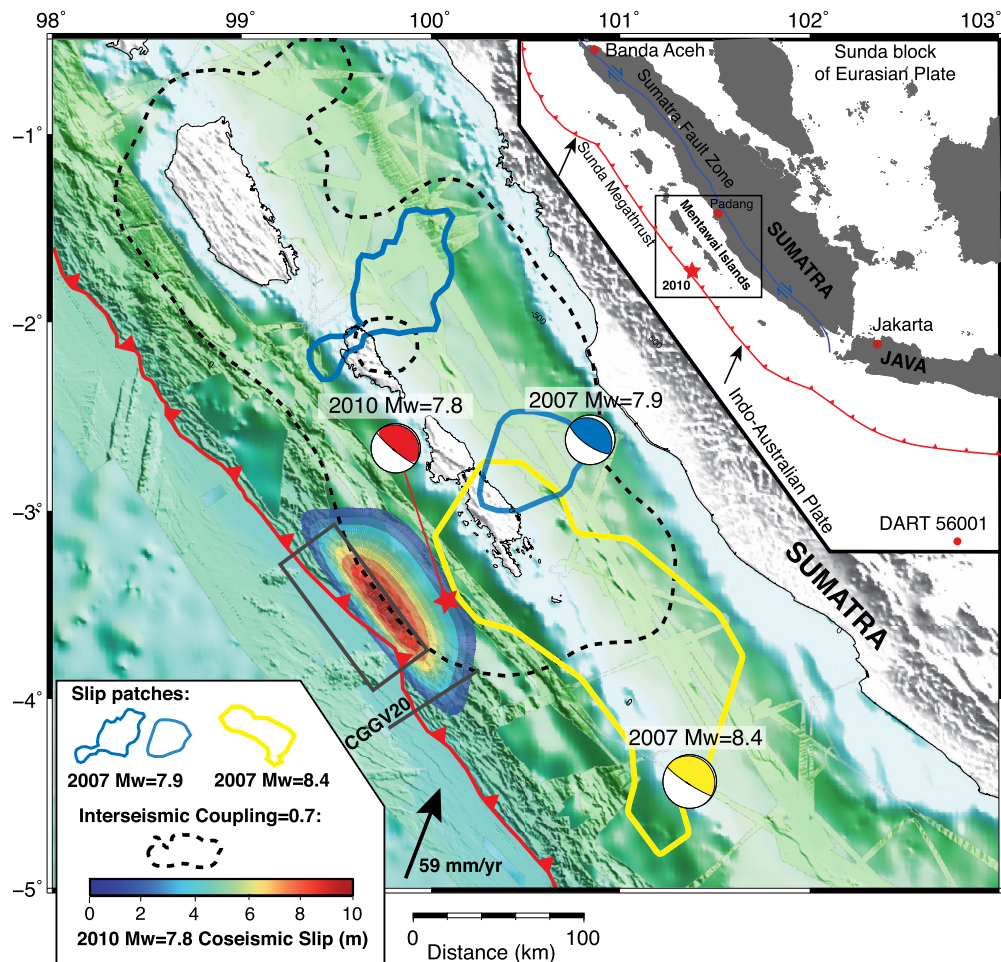


Fig. 1. Recent earthquake sources along the Mentawai segment of the Sumatra subduction zone. Black dashed contour shows the region with high (>0.7) inter-seismic, inter-plate coupling (Chlieh et al., 2008). The M_w 7.8 2010 tsunami earthquake GCMT focal mechanism and BMKG location: red beach ball and star. The preferred co-seismic slip model (colour scale) is from Hill et al. (2012). The deeper part of the megathrust ruptured in a sequence of three earthquakes in 2007 (M_w 8.4 Bengkulu main shock, M_w 7.9 Pagai-Sipora and M_w 7.0 sub-shocks, e.g. Feng et al., 2016; Konca et al., 2008). Dark grey box indicates location of the study area in Fig. 2. Dark grey line indicates location of the portion of CCGV20 profile shown in Fig. 5. Inset at the upper right corner shows regional setting of the Sumatra subduction zone. Bathymetry compilation from Franke et al. (2008). (For interpretation of the colours in the figure(s), the reader is referred to the web version of this article.)

processing sequence was used, consisting of swell noise removal, common mid-point binning at 6.25 m along track, trace editing, velocity analysis, normal move-out correction, stacking, post-stack time migration, and depth conversion. Because of the short streamer length and deep-water setting, limited constraints on velocities could be obtained from the data themselves. To circumvent this issue, a velocity model obtained from full waveform inversion of a 15-km long streamer dataset in the vicinity of the study area (Qin and Singh, 2018) was used to convert the migrated time sections into depth sections. Using a quarter-wavelength, Rayleigh criterion, the vertical resolution of the processed high-resolution seismic reflection sections is 4 m at the seafloor for a dominant frequency of 100 Hz, and increases to 6–9 m in 2500–3500 m/s velocity sediments. Lateral resolution is limited by the common mid-point spacing (6.25 m in our case); in addition, seismic migration reduces the Fresnel zone width along the direction of the profile, to optimally a quarter wavelength. However, a half-wavelength is a more realistic estimate of the post-migration lateral resolution (Lindsey, 1989). Thus, lateral resolution is 6.25 m at the seafloor down to regions of 2500 m/s velocity, increasing to 9–10 m for regions of 3500 m/s velocity. Six profiles with 6 km lateral spacing were shot within the October 2010 Mentawai earthquake rupture zone, crossing the deformation front orthogonally. The length of these profiles varied from 40 to 80 km, but only the frontal sections of two of them are shown in Figs. 3 and 4.

A Kongsberg EM302 system with a dominant frequency of 27 kHz was also used to acquire high-resolution multibeam bathymetry and backscatter data. The bathymetry data were processed using the CARIS HIPS and SHIPS software. Data quality allowed the construction of a Digital Elevation Model with grid cells of 25 m, having a vertical resolution of up to 3–4 m at a water depth of 5800 m. Backscatter data presented in Supplementary Material were processed using SONARSCOPE of IFREMER (Fig. S1).

A deep seismic profile (CGGV20) previously acquired near the eastern extremity of the 2010 earthquake rupture zone is also used (Singh et al., 2009; 2011). The CGGV20 profile was shot in 2009 using a large (9600 in³) tuned airgun source and three streamers. Details on data acquisition and processing are given in Singh et al. (2011). The final depth migrated image for the 65-km long frontal portion of profile CGGV20 is shown in Fig. 5.

4. Structures, slip and uplift at the prism's toe

The bathymetry data (Fig. 2) and two interpreted representative sections (FK05 on Fig. 3, FK08 on Fig. 4) show the frontal part of the accretionary wedge in the 2010 rupture zone. The prism consists of a set of bivergent thrust folds, 1–4 km wide and 10–30 km long, deforming the sediment pile above the 6–8° dipping main basal décollement. Two subducting bathymetric highs (ridges R1, R2) are indenting the accretionary front.

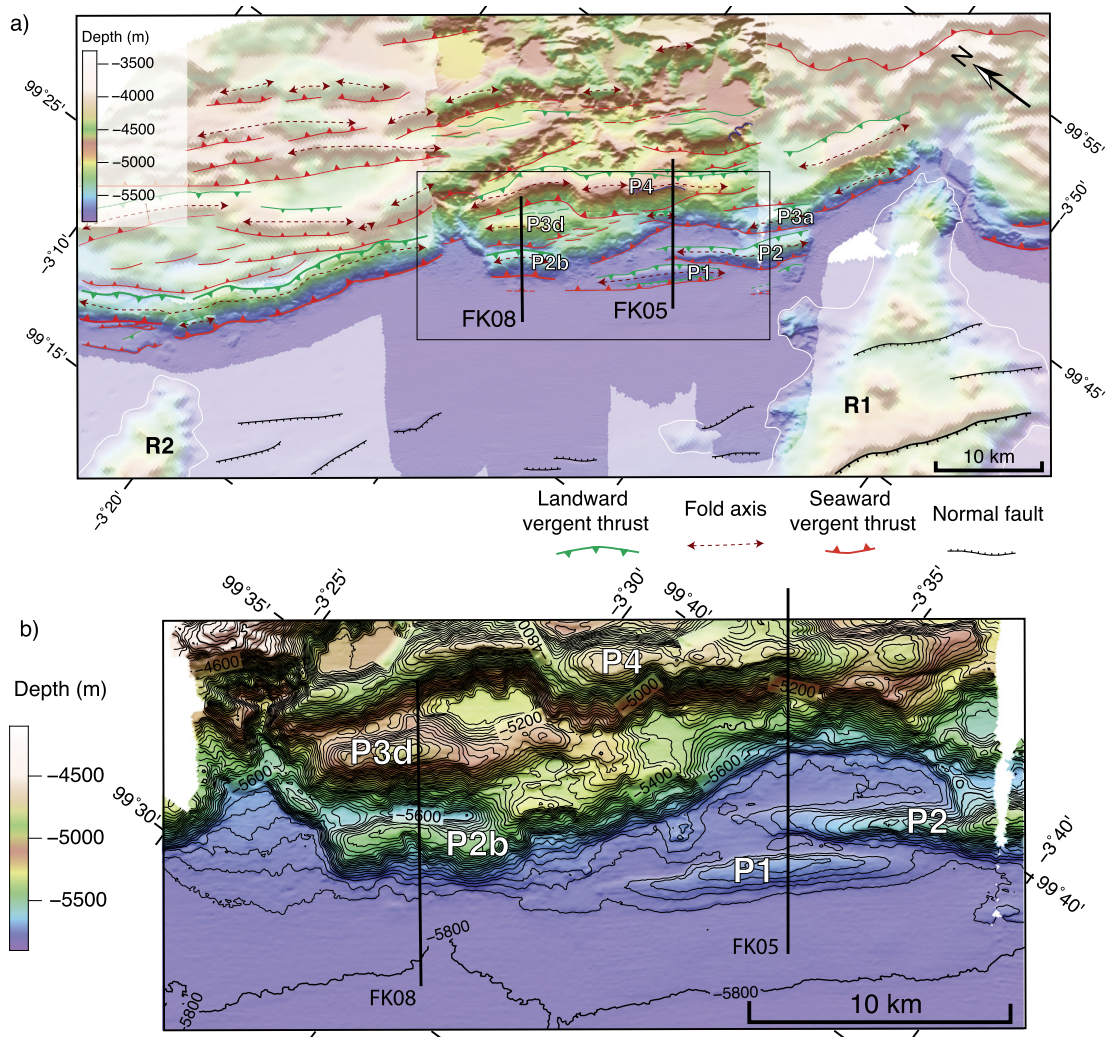


Fig. 2. Morphology of the frontal accretionary wedge in the shallow slip zone of the 2010 Mentawai tsunami earthquake. a) Interpreted bathymetry grid combines high-resolution MegaTera data (gridded at 25 m) and previously acquired bathymetry data (semi-transparent regions). Black box indicates location of (b). R1 and R2 are interpreted as two volcanic ridges on subducting seafloor. b) Close up view of accretionary wedge front (contoured every 20 m). Black lines indicate locations of portions of seismic profiles FK05 and FK08 shown in Figs. 3 and 4. P1–P4 are pop-up structures.

At a more detailed level, the FK05 profile images the subsurface structure of two frontal, bivergent thrust folds (P1, P2) at the wedge tip (Fig. 3). P1 and P2 are each bounded by a pair of thrust faults with opposite dips of 45 to 60° (landward-dipping T1_f, T2_f, and seaward-dipping T1_b, T2_b). These steep, conjugate thrusts appear to merge downwards and root either on the main décollement near the top of the oceanic crust (D1 for P1) or on a shallower décollement level within the trench turbidites (D2 for P2). The nearly flat-topped blocks they bound display the typical geometry of “pop-up” structures (numbered: P1, P2/P2b, P3a/P3d, P4; Figs. 2, 3, 4). The term “pop-up”, which usually refers to a hanging-wall block uplifted by a high-angle forethrust/backthrust pair that connect to an underlying low-angle décollement (McClay, 1992), is unequivocally best adapted to describe these nearly symmetrical structures.

On profile FK08 (Fig. 4), two thrust anticlines P2b and P3b are also observed at the front of the accretionary prism. Their forethrusts (T2b_f, T3d_f) have main dips of 30–45°, while their less prominent backthrusts (T2b_b, T3d_b), with more distributed and much smaller localised offsets, dip more steeply (60–70°). While both structures appear to be intermediate between fault-bend folds (i.e. sediment layers that remain parallel to the underlying thrust as it bends across a flat to ramp corner, Fig. 6c) and simple pop-

ups, we also refer to them in the following as “pop-up structures” for simplicity. The frontal one clearly roots at depth on the same décollement (D2) as P2 in profile FK05 (Fig. 3).

The high-resolution seismic profiles permit measuring finite displacement and uplift amounts on the pop-up bounding thrusts. Cumulative slip on the faults on either side of P1 was asymmetric, as reflected by the overall southward tilt of both the seafloor and turbidite layers (yellow and green coloured reflectors, Fig. 3). It was four times larger (≈80 m) on the seaward-dipping thrust T1_b than on the landward-dipping one T1_f (≈20 m). Slip was also asymmetric on either side of P2, but larger on north-dipping T2_f (≈80 m) than on T2_b (≈20 m). Assuming only small internal pop-up deformation and slip conservation between the décollement and the conjugate thrusts (Fig. 6b), slip on both décollements would be on order of ≈80 m. This would be consistent with the ≈60 m cumulative uplift of the seafloor atop both P1 and P2 on profile FK05. The seismic resolution of that profile is enough to estimate the youngest co-seismic seafloor uplift (≈6–8 m) across symmetrical scarps bounding the most-frontal mini-pop-up at the upper tip of T1 (Fig. 3, top left inset). We interpret such uplift, consistent with 8–11 m of surface slip on emergent thrusts dipping 40°N and 60°S, respectively, to be due to the last (2010?) or at most the last 2 seismic events.

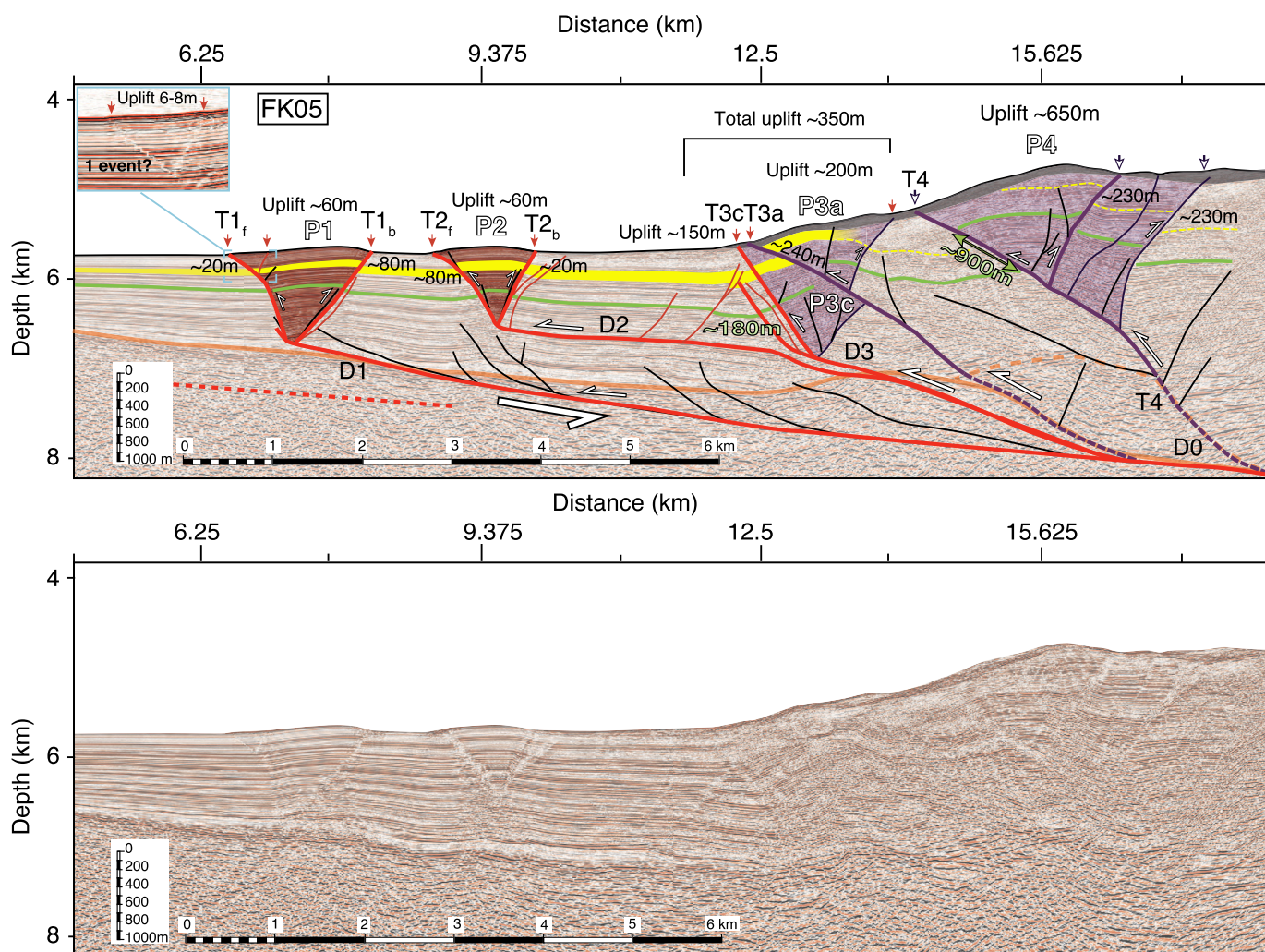


Fig. 3. High-resolution seismic reflection images across the accretionary prism front. Migrated, depth-converted section (bottom) and corresponding interpretation (top) of seismic profiles FK05 (see location on Fig. 2). Shallow-dipping, coloured lines and levels are reasonably well identified sedimentary layers (dashed where less clear). Thick red lines indicate main, youngest active thrusts, identified as active as they produce clear slope-break on the seafloor. Thick purple lines indicate main older thrusts, inferred to be older as they do not show clear slope-breaks on the seafloor, and are generally unconformably covered by superficial deposits (in grey). Thinner black lines are somewhat older or secondary thrust faults. Dashed red line indicates extrapolated décollement level. Orange line marks top of oceanic basement. Coloured "triangles" indicate Pop-up structures P1, P2/P2b, P3a/P3c/P3d and P4, bounded by bi-vergent thrust faults. Red: youngest, and purple, older active pop-ups. T1–T4: seafloor emergent thrusts. D0–D4: active décollement levels. Small red arrows identify recent seismic surface breaks. Numbers indicate total amounts of slip or uplift, as estimated from the interpreted sections using offsets of well identified (coloured) layers. Total cumulative uplift of 5 main pop-ups is indicated above section. Insert on top left shows fresh, most recent uplift of the most frontal sub-popup, likely due to the 2010 earthquake.

Farther landwards along profiles FK05, several larger pop-ups are clearly imaged (Fig. 3). Pop-up P3 is a composite, faulted structure. Its lower wedge (P3c) clearly roots into décollement D3, a northwards extension of D2 that rises gently from the main plate boundary décollement D0. The upper part of that pop-up has been cut and offset, off sequence, by ramp thrust T3a, that also connects with D0. The corresponding, truncated half of P3c (P3a), has been displaced by ≈ 240 m seaward. This composite pop-up (P3a/P3c) was uplifted by a total of ~ 350 m. Yet farther landwards, pop-up P4 appears to have resulted from conjugate thrusting at the updip of a landward-dipping ramp thrust (T4) rooting on D0. The cumulative amount of deep slip on P4's two high-angle, seaward-dipping thrusts appears to balance the total offset (900 m) on T4 (offsets of green reflector, Fig. 3 top). Note that the shallower total slip on the two steeper, northern thrusts is only 460 m (offsets of yellow-dashed reflector, Fig. 3 top). The top, shallower part of that pop-up has clearly been eroded, especially on its south side, consistent with the steeper surface slopes observed in the bathymetry (Fig. 2). Evidence for erosion is also clear from the uninterrupted, unconformable layer of superficial deposits (dark grey, Fig. 3) that

truncate both the turbidites and the tip of thrust T4. These superficial deposits are not cross-cut by T4, indicating that this structure is probably not active anymore. In spite of erosional degradation, we estimate, based on the offset on T4, that the cumulative uplift of P4 was on order of ~ 650 m.

On the FK05 section (Fig. 3), beneath pop-up P3c and décollement D3, as well as farther north, deep under P4, two similar, asymmetric bulges with deformed strata protrude upwards above what we interpret to be the uniformly shallow-dipping plate-boundary décollement. Both of these structures may be interpreted to result from shortening of the oceanic crust's basaltic layer, as inferred across the Nankai and northern Sunda trenches (Moore et al., 2009; Singh et al., 2008). A velocity pull-up effect or subduction of hidden seafloor topographic ridges, however, cannot be excluded. Profile FK08 (Fig. 4), only 12 km north-westwards, shows only one similar, albeit much smaller, bulge beneath pop-up P2b. Whatever the origin of such basement bulges, their presence might have contributed to the development of shallower décollement levels within the turbidite layers, accounting for the shallower rooting depths of pop-ups P2 and P2b. By contrast, the youngest, frontal,

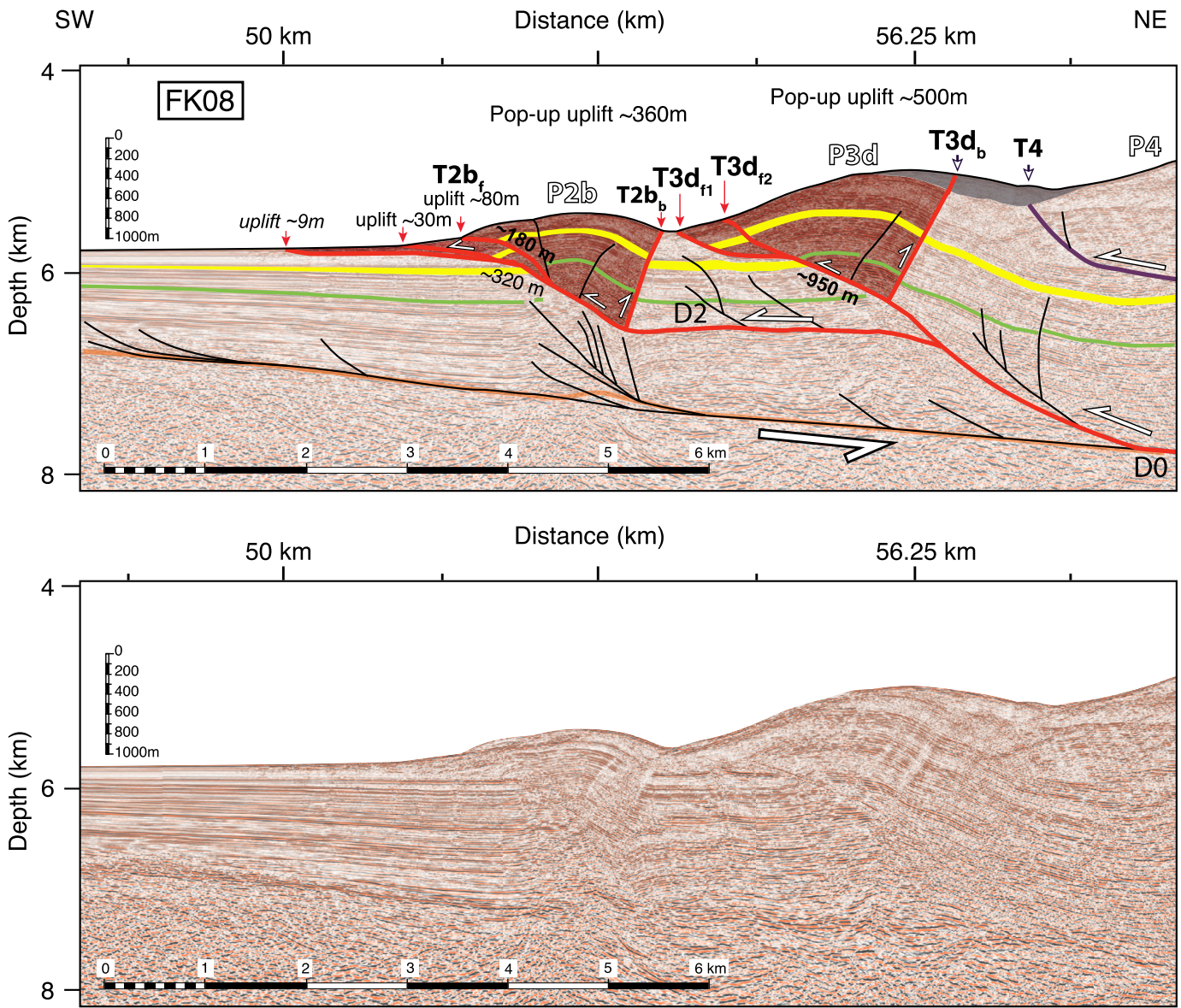


Fig. 4. High-resolution seismic reflection images across the accretionary prism front. Migrated, depth-converted section (bottom) and corresponding interpretation (top) of seismic profiles FK08 (see location on Fig. 2). Symbols and interpretation details, as Fig. 3. Pop-up P4 (Fig. 2), northwest of P3d, is bounded at its seaward tip by thrust T4, now inactive. Where crosscut by FK08, inactive pop-up P4 has been strongly eroded, leading to poor imaging. While several small, south-dipping thrusts offset beds on the north sides of P2b and P3d, such offsets are small, and both P2b and P3d are best described as fold-bend folds. Note remarkably constant dip (8.5° North) of décollement D0.

deeper rooted pop-up P1 clearly formed as a result of slip propagating on the main, plate boundary interface décollement D1 at the base of the oceanic, pelagic deposits.

On profile FK08, south of the relatively steep southern slope of P2b (Figs. 2, 4), two very shallow dipping thrusts extend up to ≈ 2 km into the superficial trench deposits. Hanging wall deformation associated with both clearly reach the surface, and the corresponding more seaward and landward cumulative uplifts are ≈ 9 and 30 m, respectively (Fig. 4). The surface trace of the next thrust northwards is marked by a steeper bathymetric uplift of up to 80 m. Pop-up P2b is well developed and shows negligible superficial erosion. Clear cumulative offsets, mostly on the landward dipping thrusts on its south side, match more distributed thrusting and folding on its north side, and amount to a total 500 m, in keeping with a total uplift of ~ 360 m. Such uplift, which is much larger than the summed uplifts of frontal pop-ups P1 and P2 on FK05, is comparable to that of P3a. This is consistent with the broad-scale morphology on the bathymetry (Fig. 2). Like P2 and P3c on profile

FK05, P2b appears to root on a décollement level (D2) within the near horizontal trench turbidites. Remarkably, the corresponding total slip on that décollement on profile FK08 (≈ 500 m) would be the same as that on D0 south of T4 on profile FK05 (Figs. 3 and 4). Significant thrusting and deformation within the lower part of the turbidite pile beneath P2b implies that the deeper, plate-interface décollement D0 has already propagated under P2b, and farther seaward. Hence, as observed on profile FK05, there is evidence on profile FK08 for two superimposed décollement levels at comparable depths. Farther landwards, pop-up P3d, which is larger than P2b, is associated with a total uplift of ~ 500 m. The landward-dipping thrust T3d has offset the green reflector by ~ 950 m. Like that of P4, the southern, steeper slope of P3d shows clear signs of erosion, although surface reaching thrusts T3d_{f1} and T3d_{f2} appear to be still active. Note finally that the average sizes, simplified geometry (pop-up/fault-bend fold intermediate structures), overall uplift, and total offset amounts on landward dipping thrusts of P3d and P4 are closely comparable, as suggested also by their relative

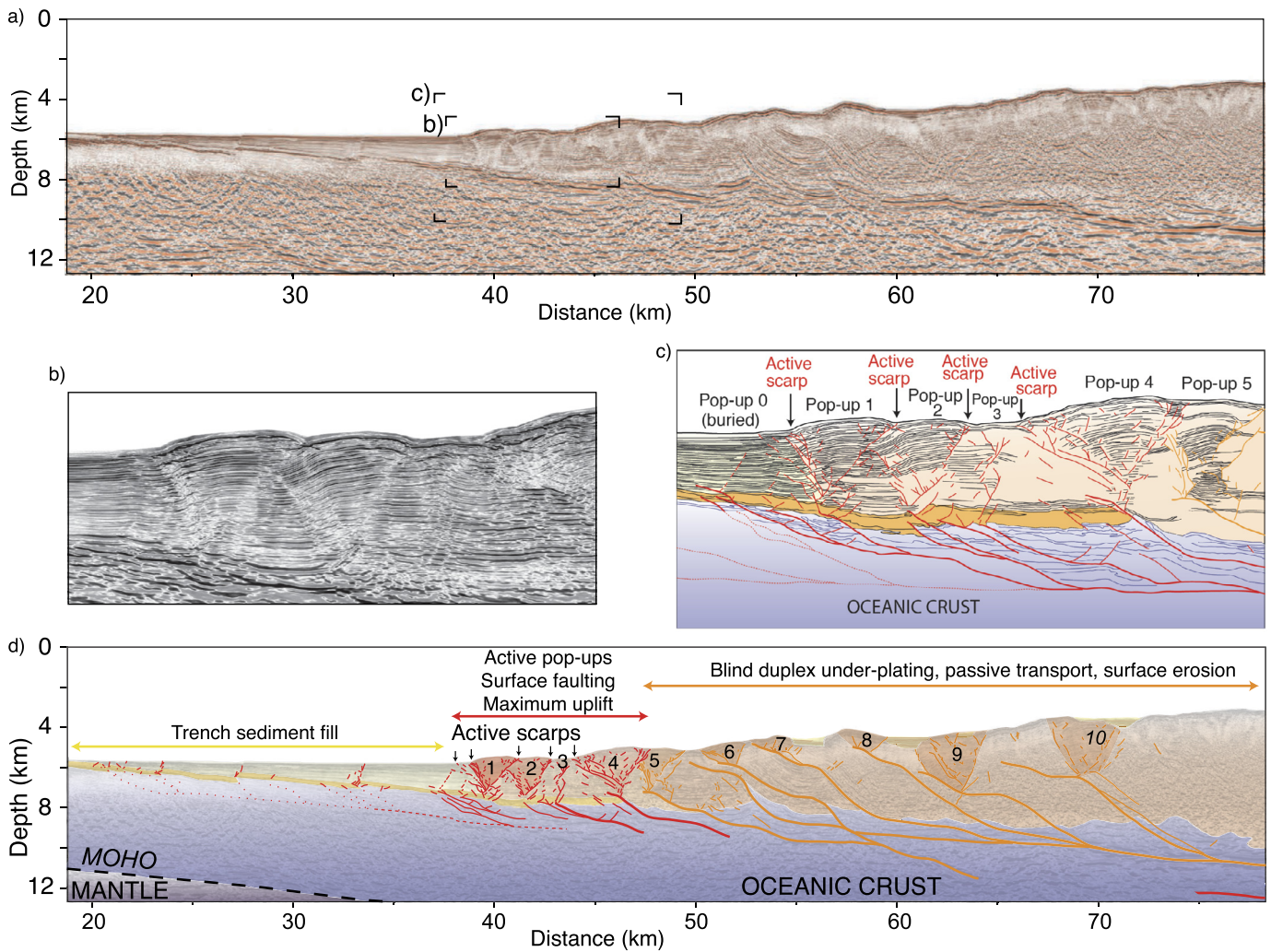


Fig. 5. Deep seismic reflection image (a) and tectonic interpretation at crustal scale (d) of depth migrated CCGV20 profile, located near southeast tip of 2010 earthquake rupture (located in Fig. 1), modified after Singh et al. (2011). b) and c) show data and interpretation of enlarged section of accretionary front (located in a). Shallow pop-up structures (1–10) and deeper fault-propagation folds are clear over an accretionary width of ≈ 35 km. Oceanic crust is blue. Undeformed and thickened trench turbiditic deposits are pale yellow. Thin yellow layer (light orange in c) represents older pelagic sediments, characterised by high-amplitude negative polarity reflection beneath turbidites. Frontal pop-ups 1 to 4 (shaded red), bounded by conjugate, seafloor-emergent reverse faults that root into shallower dipping thrusts offsetting top oceanic crust, appear to be actively uplifting, in contrast with pop-ups 5 to 10 (shaded orange) that seem inactive, as partially eroded.

positions and topographic signatures on the seafloor morphologic map (Fig. 2b). This implies remarkably similar growth histories in general, but with some recent twists in frontal propagation mechanics.

In the rupture area of the Mentawai 2010 tsunami earthquake, convergence is therefore accommodated along distinct, localised tectonic structures. Slip along the décollement is transferred to bivergent thrust faults bounding flat-topped pop-ups or fault-bend folds. Both forethrusts and backthrusts accommodate convergence through slip/bending and therefore flat seafloor uplift in between, on time scales long enough to grow to widths of 2 to 3 km. The measurements made on the interpreted seismic profiles indicate that the amount of long-term uplift of the pop-ups is ≈ 70 –85 % of the slip accumulated by the thrusts. That ratio is slightly smaller ($\sim 50\%$) for the fault-bend anticlines (e.g., P3d). Yet, the amount of uplift generated by these structures is much larger than that which would result from similar amounts of horizontal slip on the 6–8° dipping décollement alone (only about 10% of that slip).

Pop-up structures have already been imaged and interpreted along other segments of the Sunda trench (Singh et al., 2008; 2011; Bradley et al., 2019). South of our study area, the deep seismic reflection profile CCGV20 (Fig. 5, location on Fig. 1) shows

particularly well the geometry and kinematic timing of such structures. There, the wedge attains a maximum thickness of ~ 8 km, and more than 10 pop-ups can be identified up to ~ 40 km north of the trench axis. They are 2–3 km wide and spaced mostly from ≈ 0.5 to ≈ 3 km. They have clear triangular shapes, with gently folded lateral limbs bounding wide, horizontal, central plateaus. They are bounded by 2 main bivergent thrust fault zones that merge downdip where they branch off shallower-dipping, deeper thrusts that rise from the master plate-boundary décollement within the upper oceanic crust. Farther landwards, the pop-up bases rise to the tips of deeper thrusts that shorten the base of the thicker accretionary prism, a geometry similar to that described farther north (Kuncoro et al., 2015). The pop-up crests are gradually more eroded landwards. Only the thrusts bounding pop-ups 1, 2 and the front of pop-up 4, that appear to offset the seafloor, are likely active. South of pop-up 1, minor, localised faulting in the trench turbidites, may reflect the inception of future pop-ups.

The results of most studies of the 2010 Mentawai earthquake, based on different datasets, all concur to suggest that a very large amount of slip near the trench on a low dipping décollement is required to generate high seafloor uplift and the observed tsunami wave-heights. However, the new seismic data show the existence

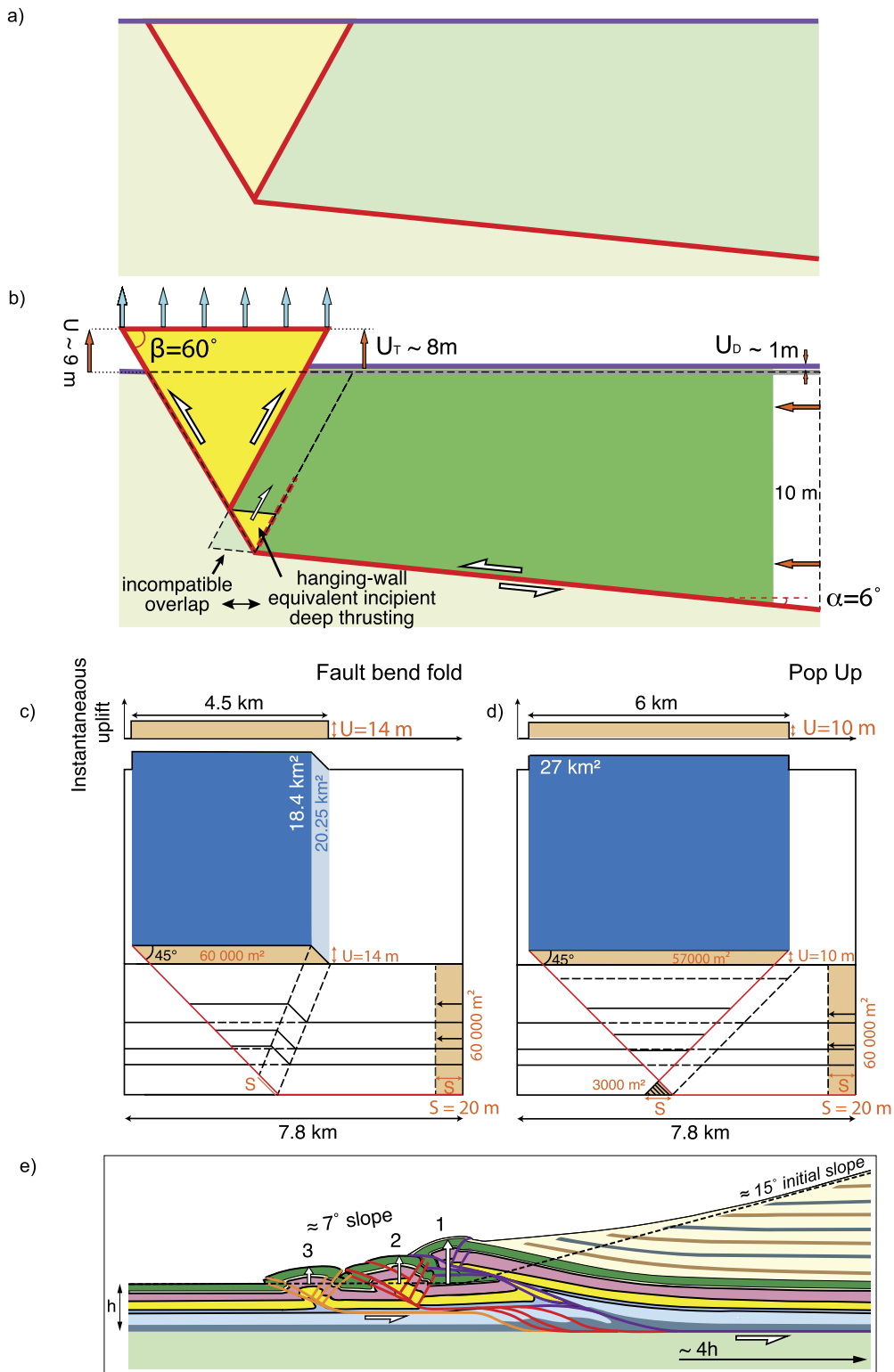


Fig. 6. Geometry and faulting/uplift of pop-up structures. (a) Initial triangular geometry of 60° , landward- and seaward-dipping thrust faults bounding Pop-up at frontal terminus of decollement. (b) ≈ 9 m seafloor uplift due to 10 m co-seismic, horizontal shortening and ≈ 10 m slip on shallow, 6° - dipping decollement. Note that co-seismic uplift above decollement is only ≈ 1 m. Strong hanging-wall shortening of prong at decollement/Pop-up tips bend leads to basal, upper-plate back thrusting (c, d) Identical shortening and thrust dips produce broader seafloor uplift by pop-up extrusion than by fold-bend folding. (e) Example of Pop-up uplift in analogue "sand-box" experiment, over-drawn on top of Fig. 5-b in Konstantinovskaya and Malavieille (2011): high-friction basal layer (light green), taken here to represent Oceanic crust, is topped by a low-friction (glass micro-beads) decollement level. Bottom sedimentary layers (dark and light blue) are inferred to correspond to pelagic, oceanic deposits. Coloured sand layers above (yellow, pink, green) are taken here to represent trench turbiditic sediments. Other layers (top right side of model) are considered to belong to more stable, passively transported, accretionary wedge. Successive Pop-ups, younging towards the left, are bounded by distinct, conjugate thrusts (blue, red, yellow). Note predominant, left-directed overthrusting and multiple, smaller, conjugate thrusts with opposite dips. Vertical arrows show cumulative pop-up uplifts. Dashed black line represents initial position of model top surface ("Seafloor"). Horizontal, long black arrow is total basal displacement at that stage of the model. Successive thrust and ramp lines young from blue to yellow.

of frontal, actively rising pop-ups near the prism toe that may account for a high ratio of seafloor uplift as a result of sub-horizontal co-seismic slip. As elaborated below, the forced transfer of such slip at the terminus of the megathrust basal décollement to sub-vertical, upward pop-up extrusion may promote very large amounts of seafloor uplift (Fig. 6a, b). Highly reflective back-scatter signals on both sides of the frontal pop-ups in the 2010 rupture area might support recent surface ruptures due to such uplift (Fig. S1).

5. Seafloor uplift associated with co-seismic, vertical pop-up extrusion

Here we describe the mechanism through which pop-up structures can generate high seafloor uplift. The simple diagrams in Fig. 6(a, b) show how instantaneous vertical uplift arises from co-seismic rupturing of steep thrusts bounding a pop-up structure at the terminus of a near-horizontal décollement. How slip on the décollement translates into vertical pop-up uplift depends on the dip of its bounding thrusts.

Assuming uniform horizontal displacement (hc) atop a décollement with dip-angle (α), slip on the décollement (S) is:

$$S = \frac{hc}{\cos(\alpha)}$$

The uplift U_D generated by such slip is:

$$U_D = S \times \sin(\alpha)$$

Assuming conservation of movement, the frontal pop-up is extruded upward by slip on the frontal ramp-thrust dipping at an angle β . The corresponding pop-up uplift is:

$$U_T = \frac{S \times \sin(\beta - \alpha)}{2 \cos(\beta)}$$

Detailed calculation of this uplift is provided in the Supplementary Material.

The total seafloor uplift generated by both motions is:

$$U = U_D + U_T = \left(\sin(\alpha) + \frac{\sin(\beta - \alpha)}{2 \cos(\beta)} \right) \times \frac{hc}{\cos(\alpha)}$$

For bounding ramp thrusts dipping 45° to 60° , as generally observed on the seismic sections, the corresponding vertical pop-up uplift would thus be on order of 45 to 81% of the horizontal slip. As illustrated on the simplified, realistic section of Fig. 6b, 10 m of horizontal displacement of the upper plate would result in 10.06 m of slip on a 6° -dipping décollement, and produce 8.14 m of vertical uplift of a pop-up bounded by 60° -dipping ramp thrusts. Such uplift would be nearly 8 times larger than that (1.05 m) of the wedge atop the décollement. The total uplift of the pop-up above the undeformed trench seafloor would be 9.19 m, a value very close to the 10 m horizontal slip of the upper plate. In such a simple model, with symmetrical pop-up forethrust and backthrust slip, an amount of seafloor uplift almost equal to the co-seismic slip on the plate-interface décollement would be transferred to the entire top width of the pop-up plateau, maximizing the transmission of co-seismic deformation to deep water. The main parameter impacting the amount of pop-up uplift is the dip of its conjugate bounding thrusts, which controls the trade-off between upper plateau width and uplift (Fig. 6d).

Other models of hanging wall deformation at the tip of the plate interface décollement differ mostly by the strain styles near the sharp bend between the décollement and the sea-vergent thrust. Fault-bend fold and fault-propagation fold models assume that such bending is taken up by kink-band like shear, distributed

over a fairly broad, linear, conjugate zone extending all the way to the surface (Fig. 6c). That deformation style resembles what is observed on profile FK08 (Fig. 4). Different types of corner bending deformation, classically observed in sandbox experiments (Fig. 6e) include strong, localised shortening of the overlapping hanging-wall tip, resulting in the birth of a new, deep, conjugate backthrust (Figs. 6b, e). Models of instantaneous seafloor uplift for a fault-bend fold (Fig. 6c) and a pop-up (Fig. 6d), that are the most relevant for the structures observed here, result in similar conversion of décollement slip into seafloor instantaneous uplift (see other scenarios of instantaneous uplift for different fold types in Hubert-Ferrari et al. (2007) and references therein), but we note that kink-bands are steeper than pop-up back-thrusts, producing narrower uplifted surfaces as slip propagates across a fault-bend fold than across a pop-up. Therefore, pop-up structures are particularly efficient to generate large uplift over wide areas.

In any event, whatever type of model is found more adequate, the accretionary front seismic profiles (FK05, FK08) support the inference that the sudden vertical uplift of the seafloor and overlying water-column associated with the upwards expulsion of a few sub-parallel pop-ups is a particularly efficient mechanism for triggering a large tsunami.

As shown in analogue models of fold-and-thrust belts, the formation of pop-ups is governed by the mechanical properties of underlying décollements (e.g. Graveleau et al., 2012). Strong basal friction leads to the formation of asymmetric, imbricate slices separated by low-angle thrusts. Weak basal friction produce symmetrical folds bounded by high-angle thrusts (e.g. Malavieille and Konstantinovskaya, 2010), as is common in fold-and-thrust belts detached atop viscous layers such as evaporates (Costa and Vendeville, 2002), and in keeping with “Critical Taper” prediction of steep thrusts with no preferred vergence, hence common backthrusts, atop a weak basal layer (e.g. Davis and Engelder, 1985).

Fig. 6d, derived from Fig. 5b in Konstantinovskaya and Malavieille (2011), shows an interpreted cross-section of the early stage of a sandbox experiment where a high-friction basal layer moves below a low-friction décollement at the base of layered sediments. While that snapshot was extracted from successive stages of an analog model designed to simulate exhumation in orogens, it illustrates remarkably well the growth of structures similar to those imaged by seismic sections across the Mentawai accretionary front. Specifically, it shows that the steep ramp-faulting that drives pop-up uplift is asymmetric, with large fore-thrusts and multiple back-thrusts that develop at the décollement/ramp corner, before being more passively uplifted. It clearly shows how most of the surface uplift is driven by pop-up extrusion (Fig. 6e, arrows 1, 2 and 3). It illustrates how active décollement levels can rise from one weak depositional interface to another, as apparent in profiles FK05 and FK08, and how most pop-ups, which do not generally overlap, reach a critical amount of vertical extrusion – on order of their half-width – before being superseded by smaller, more frontal one (Fig. 6e). Also, discrete, successive back-thrusting, rather than kink-band shear, is observed to compensate the frontal impactation of the hanging-wall lower wedge-tip (dashed triangles on Figs. 6b and d, and dashed red line in Fig. 6b). In short, that experiment faithfully reproduces most of the small structures imaged in profiles FK05 (P1, P2, P4, Fig. 3) and CCGV20 (Fig. 5).

6. Contribution of pop-ups in tsunami generation during the 2010 Mentawai earthquake

To test the idea that additional uplift in deep water resulting from co-seismic rupturing of pop-up structures could significantly enhance tsunami waves, we performed tsunami simulations for the 2010 Mentawai earthquake.

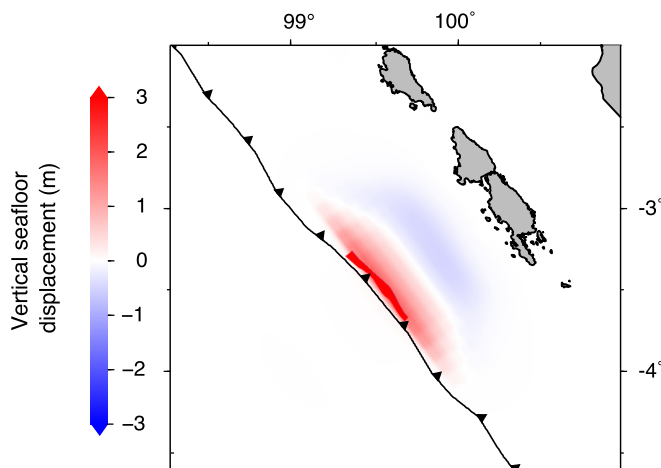


Fig. 7. Vertical seafloor displacement used to initiate tsunami modelling. Initial surface elevation combines the uplift contribution of pop-up structures, shown here for the reference region of $60 \text{ km} \times 6 \text{ km}$, and seafloor deformation for the 2010 Mentawai tsunami earthquake calculated from the preferred slip distribution of Hill et al. (2012) without sediment effect.

Modelling was carried out using a fully nonlinear Boussinesq wave model (FUNWAVE-TVD, Shi et al., 2012) to simulate the wave propagation and inundation process, a model suitable to simulate tsunami waves generated by small-scale sources that commonly have short wavelengths and a dispersive character. FUNWAVE has been extensively validated using tsunami benchmark tests (Tehranirad et al., 2011) and widely applied to real-scale tsunami events (Tappin et al., 2014; Li et al., 2015). In details, we used a 100 m grid for wave propagation simulation in the deep ocean. A nested grid approach is adopted to simulate the inundation and run-up process in four selected areas on the shores of the southern Mentawai Islands (Fig. S2), with 20 m cell size for the finest grid. The topographic data were taken from the NASA Shuttle Radar Topographic Mission (SRTM) with 3-arcsecond resolution ($\sim 90 \text{ m}$) with correction made for areas of interest using topographic information collected during field survey. The bathymetric data were derived from the following sources: (1) Digitized nautical charts for water depths up to 200 m; (2) 30 arc seconds General Bathymetric Chart of the Oceans (GEBCO) data. In addition, the Mega-Tera grid provided bathymetry data in the rupture zone of the earthquake.

First, we calculated synthetic tsunami waveforms at the location of DART buoy 56001, for different seafloor displacements. The seafloor displacement is a combination obtained by adding the uplift contribution of the most frontal region (i.e. the pop-ups, called “frontal source” in the following) to the seafloor displacement caused by slip on the megathrust (Fig. 7). The latter seafloor displacement is the one calculated by Hill et al. (2012) based on their earthquake source model, without taking into account the sediment effect. They obtained a seafloor displacement by using a forward model with Green’s functions for a horizontally layered crustal elastic crust (Wang et al., 2003).

To constrain the possible range of sizes of the frontal source region that could adequately explain the 2010 tsunami amplitude, we calculated tsunami waveforms at DART station 56001 using different frontal source geometries, whose seaward edge follows the trench axis. The geometries are determined thanks to our knowledge of the Mentawai accretionary front described above, and of the 2010 earthquake. The frontal source region is centred on the high-slip patch in the slip model of Hill et al. (2012). In the along strike direction, the area where the better-developed pop-ups were imaged is $\sim 30 \text{ km}$ long (Fig. 2). Bradley et al. (2019) recently described similar pop-up structures extending up to 40 km north of

ridge R2, which attests for the existence of a long pop-up belt along the 2010 rupture area. We therefore tested the tsunami model for frontal source region lengths of 30, 40 and also 60 km (Fig. 8a), this latter value corresponding to the distance between ridges R1 and R2 (Fig. 2). The pop-ups described above are 1–3 km wide. At least two to three sub-parallel pop-ups appear to be active, and may have ruptured in the recent event (corresponding roughly to a total width of 3–9 km). The width of the frontal source area was therefore varied from 3, to 6 and 9 km (Fig. 8b). The scale of the combined tsunami source region (the frontal one and that generated by slip on the megathrust) is $\sim 100 \text{ km}$ long parallel to the trench and $\sim 50 \text{ km}$ wide along dip, which ensures the validity of using the shallow-water wave equations.

The amount of seafloor uplift of the frontal source area depends on the slip on the décollement, modelled between 10 m and up to 23 m (Hill et al., 2012; Yue et al., 2014 respectively). The slip propagates and distributes along the 45° to 60° dipping thrusts and uplift the pop-ups (Figs. 3, 6) by an amount tested between 4 and 16 m, depending on the number of pop-ups. For instance, a slip value of 20 m on the décollement would correspond to 10 m of seafloor instantaneous uplifts of a belt composed of two pop-ups bounded by 60° dipping thrusts (over $\sim 6 \text{ km}$). The possible elastic deformation of the wedge associated with coseismic slip on the backthrusts and forethrusts of the pop-ups is not considered here.

A subset of the tsunami simulation results is plotted in Fig. 9. Comparisons between synthetics and DART signal show that relatively narrow frontal source strips with length ranging between 40 km and 60 km, width ranging between 3 km and 9 km, and uplift values larger than 8 m can produce tsunami waveforms comparable with the recorded signal. A combination of a narrower source sliver with higher uplift produces results similar to those resulting from a wider source region and lower uplift (compare, for instance, the results of source $40 \text{ km} \times 3 \text{ km} \times 16 \text{ m}$ in light blue, and of source $40 \text{ km} \times 6 \text{ km} \times 8 \text{ m}$ in dashed green).

Three tested sources yield a particularly good fit to the peak amplitude of the DART station 56001 signal (Fig. 9). When compared with published values, these results show that our tsunami simulations can model equally well the peak amplitude of the tsunami. The best source regions’ geometries are 6 to 9 km wide, involving 2–3 pop-ups along a $\geq 40 \text{ km}$ long belt, with uplifts generated by 20–24 m slip on the décollement ($60 \text{ km} \times 6 \text{ km} \times 10 \text{ m}$; $40 \text{ km} \times 6 \text{ km} \times 12 \text{ m}$; $40 \text{ km} \times 9 \text{ km} \times 8 \text{ m}$). Two other tests also lead to results slightly better than Hill et al.’s tsunami simulation involving slip on the décollement of about 16 m ($40 \text{ km} \times 3 \text{ km} \times 16 \text{ m}$; $40 \text{ km} \times 6 \text{ km} \times 8 \text{ m}$).

We further used the best-fitting frontal source ($60 \text{ km} \times 6 \text{ km} \times 10 \text{ m}$) to examine whether our proposed combined seafloor displacement model could reproduce the surveyed wave heights in the southern Mentawai Islands reported in Hill et al. (2012). The comparison of simulated tsunami wave heights with field survey measurements (Fig. 10) shows that our model is successful in producing a large tsunami, of the type generated by the 2010 event. The fits to observed tsunami run-up heights are similar or at places better than those of models invoking inelastic folding of sediments (Hill et al., 2012). Our simulations and results thus tend to show that pop-up structures can play a significant role in generating unexpectedly large tsunami waves.

In these simulations, we considered that the seafloor uplift translates into the sea surface displacement without attenuation, a valid assumption when the earthquake rupture speed is much larger than the tsunami wave propagation (Okada, 1985) and the tsunami source wavelength is much wider than the water column thickness (Saito and Furumura, 2009). This assumption was also made in the different studies of the 2010 Mentawai earthquake and tsunami with whom we compared our results earlier (e.g. Hill

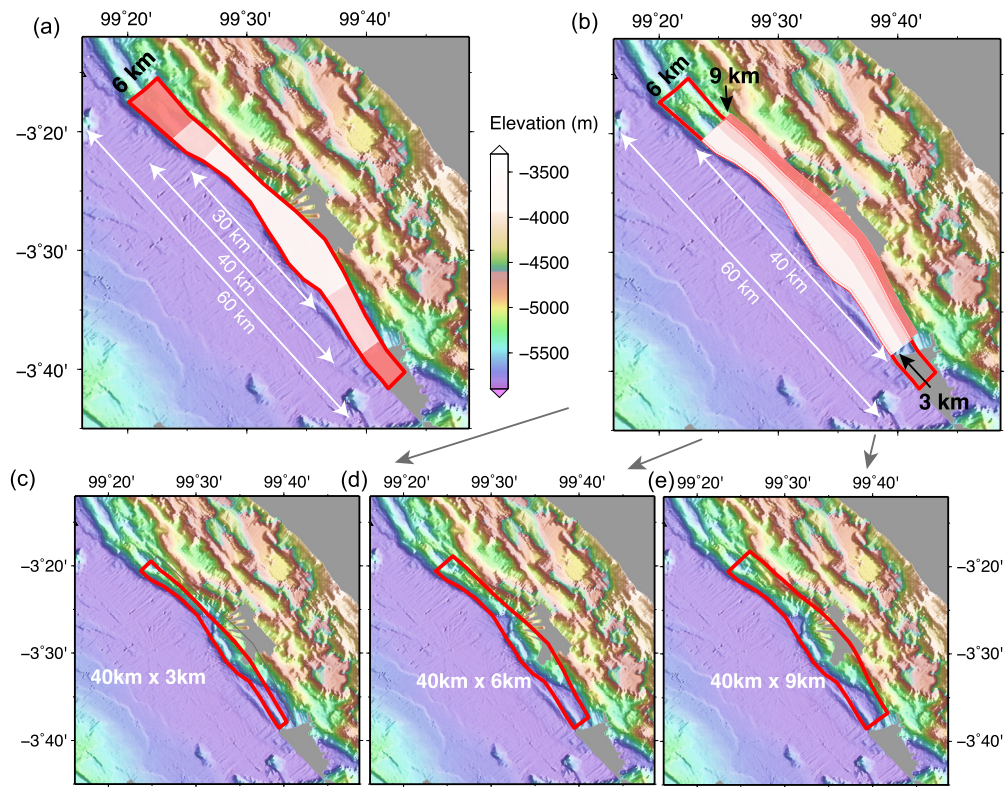


Fig. 8. Different sizes of frontal source regions tested in tsunami simulations. Polygons with filled colours have (a) different length: 30 km, 40 km and 60 km, and b) different widths: 3 km, 6 km, and 9 km. The polygons in (b) are shown separately in (c) 40 km × 3 km; (d) 40 km × 6 km; (e) 40 km × 9 km.

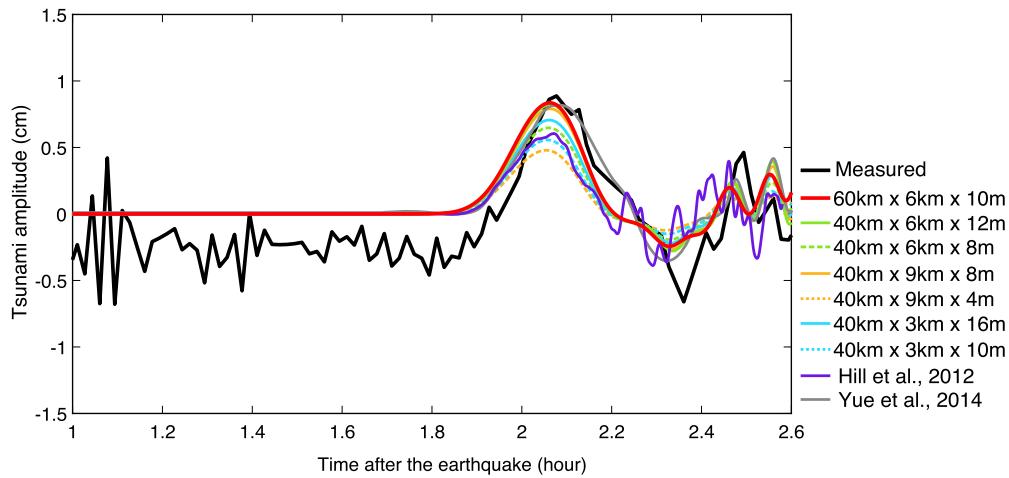


Fig. 9. Tsunami modelling results for the DART station 56001 (at 13.961°S, 110.004°E). Black line shows measured waveform, coloured lines show synthetic tsunami waveforms calculated for different frontal source region sizes and uplift values. They are compared to Hill et al. (2012)'s synthetic tsunami waveform calculated taking into account sediment effect (in purple), as well as to Yue et al. (2014) modeling (in grey). Location of the buoy is situated in Fig. 1, ~1600 km southeast of the 2010 earthquake epicentre. Note that solid red, green, and yellow models yield best fit to DART measurements (see text).

et al., 2012; Yue et al., 2014, Figs. 9 and 10). However, if these two conditions are not met, an attenuation effect (also called Kajiura filter) can reduce the sea surface displacement with regard to the seafloor uplift. In our case, such phenomenon does not apply on the broad-scale uplift generated by the slip on the décollement, which is entirely transmitted to the water column because the source is much wider than the water depth (5 km). However, attenuation might exist for the uplift generated by the frontal source only, the width of the pop-up belt (3–9 km) being similar to or roughly twice the water depth. Therefore, we tested the attenuation effect based on Saito and Furumura (2009)'s work for the different pop-up belt geometries (60 km × 6 km, 40 km × 9 km,

40 km × 6 km, 40 km × 3 km) located at 5 km depth. We found that the amount of seafloor uplift transmitted to the water column is sensitive to the width of the pop-up belt, not to the length. The wider the source, the more seafloor uplift is transferred to the sea surface. When the frontal source is the wider (9 km), the sea surface displacement equals 50% of the uplift generated by the pop-up belt (Fig. S3, or about 60% of the total seafloor uplift), a value that is reduced to about 27% and 3% for the 6 and 3 km wide frontal sources, respectively (or to 40 and 20% of the total seafloor uplift respectively). Thus, even if an attenuation effect applies, simultaneous activation of several pop-ups is needed to generate a high tsunami wave at the surface. In this case, and even if the sea sur-

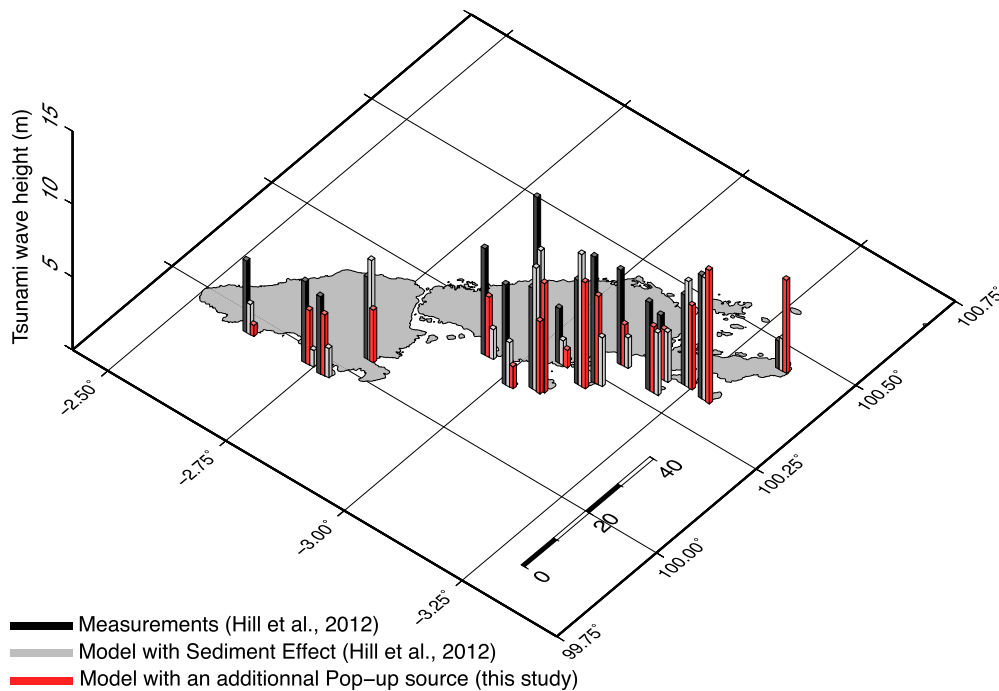


Fig. 10. Comparison of tsunami run-up heights in the southern Mentawai Islands. Observed tsunami run-up heights (black), modelled run-up heights from Hill et al. (2012) (model with sediment effect, light grey) and modelled run-up heights using uplift contribution of pop-up structures (red, this study).

face displacement equals maximum 60% of the total seafloor uplift, pop-up structures still have the ability to promote higher sea surface displacement than that solely generated by the slip on the megathrust.

7. Occurrence of pop-ups and tsunami hazard

Though infrequent, tsunami earthquakes have been identified at a number of subduction zones, such as Japan (1896), Alaska (1946), Hikurangi (1947), Kuril (1963, 1975), Nicaragua (1992), Peru (1960, 1996), Java (1994, 2006) and Sumatra (Nias-Simeulue 1907, Mentawai 2010) (Kanamori, 1972; Pelayo and Wiens, 1992; Abercrombie et al., 2001; Ammon et al., 2006; Kanamori et al., 2010; Bell et al., 2014; Kanamori and Kukuchi, 1993). They occur in a variety of settings, from erosional to accretionary trenches. Their occurrence, as that of smaller-magnitude, long duration events on the shallow segments of megathrusts has not been conclusively linked to one or more subduction parameters (El Hariri et al., 2013). Great subduction earthquakes rupture much wider down-dip portion of the seismogenic zone, and slip in the up-dip region may be triggered by large slip at greater depths (Ide et al., 2011). Given the limitations in assessing the coupling status of the shallowest parts of megathrusts (Almeida et al., 2018), and in view of recent geological evidence for ancient “slip-to-trench” events (Vannucchi et al., 2017), it is prudent to assume that many up-dip segments of subduction zones worldwide might rupture co-seismically during tsunami earthquakes (Hubbard et al., 2015).

Together, the 2007 sequence and 2010 earthquake ruptured only part of the Sunda Mentawai segment, while the region between 0.5°S and 3°S, quiet since the great events and tsunamis of 1797 and 1833, has accumulated ~8–10 m of slip deficit and is now highly-coupled (e.g. Sieh et al., 2008). Events with long rupture times, suggestive of tsunami earthquakes source conditions, have occurred north of the 2010 rupture (Bilek et al., 2011), in an area with mixed-vergence thrusts that may have ruptured in 2010 (Bradley et al., 2019). One deep seismic profile across the 0.5°S–3°S seismic gap (Kuncoro et al., 2015) shows clear frontal pop-ups, implying that tsunamigenic ruptures could be expected there,

threatening the Mentawai and populated coast of West Sumatra. As suggested by our results, such near-trench pop-ups could amplify tsunami waves generated by future events in the remaining Mentawai locked patch. Farther southeast, the Java trench, offshore the most populated part of Indonesia, has produced two recent tsunami earthquakes (in 1994 and 2006) and might generate larger ones in the future, which requires further detailed studies of the links between accretionary tectonics and tsunami-generation.

Rupture of splay faults within the wedge and anelastic sediment folding at the toe are commonly advocated for generating additional seafloor uplift leading to large tsunamis (disproportionately large in the case of tsunami earthquakes). Uplift of pop-up structures, which may be viewed as one case of multiple splay activation near the wedge toe, quantitatively relates vertical pop-up roof uplift to frontal slip on the megathrust. Pop-ups, that typify wedge growth by frontal accretion of “lower plate” sediments, must thus play a key role in tsunami generation along trench segments showing mixed-vergence frontal structures. This is the case of parts of Alaska (von Huene et al., 2012), Cascadia (Yelisetti et al., 2017), Nankai (Moore et al., 2011), southern Hikurangi (Barnes et al., 2010), Sumatra (Kuncoro et al., 2015), and along the Mentawai trench (Bradley et al., 2019). Multi-beam bathymetry and high-resolution seismic imaging should help detect pop-ups and hence better assess tsunami hazard.

8. Conclusion

Slip distribution models of the M_w 7.8, 2010 Mentawai tsunami earthquake, offshore south-central Sumatra, require that the large tsunami wave following that event was generated by a narrow swath of high seafloor uplift along the accretionary wedge front (Hill et al., 2012; Satake et al., 2013; Yue et al., 2014). This implies much higher vertical throw than that simply associated with slip on the shallow-dipping Sunda megathrust, suggestive of additional mechanisms. New high-resolution seismic reflection and bathymetric data acquired across the 2010 rupture zone yield an unprecedented overview of the deformation front, and help quantify its contribution to such higher-than-expected uplift.

The accretionary front along the relatively narrow 2010-Tsunami-earthquake source area is characterized by steeply-dipping active thrusts that branch upwards from the subduction megathrust and bound triangular pop-ups, a geometry that is classically observed in analogue sand-box models of fold-and-thrust belts in the hanging walls of décollements with weak basal friction.

Simple trigonometry is used to constrain a model that quantifies vertical pop-up uplift as a function of horizontal shortening. The determined co-seismic slip (10–15 m) on the 6°-dipping décollement likely caused a comparable amount of upward expulsion of the observed, 3–6 km-wide, flat-topped pop-ups. Co-seismic throw on the ≈60° dipping thrusts can thus maximize the uplift of the seafloor and overlying water-column, providing strong, localised tsunami sources.

We tested this model by running tsunami simulations of the Mentawai 2010 event considering a composite source integrating the uplift generated by slip on the megathrust and the uplift generated by the vertical expulsion of the pop-up belt. The peak amplitude of the 2010 tsunami recorded by the DART 56001 buoy is best-fit for a deformation involving 8–10 meters of seafloor uplift across a 6 to 9 km-wide and 40–60 km long pop-up belt (corresponding to up to three parallel pop-ups). Such a scenario also satisfactorily reproduces the run-up heights in the Mentawai Islands.

We propose that such a simple mechanism is efficient to generate the oversize waves that characterize Tsunami-Earthquakes. Such structures have been identified at different places along the Sumatra-Andaman accretionary wedge, and should be looked for along other convergent margins in order to identify trench segments prone to produce this special class of seismic events that spawn exceptionally large tsunamis.

Declaration of competing interest

The authors declare that they have no known competing financial interests or personal relationships that could have appeared to influence the work reported in this paper.

Acknowledgements

The Mega-Tera experiment is an international project between the Earth Observatory of Singapore (EOS), the Indonesian Institute of Sciences, Schmidt Ocean Institute (SOI) and the Institut de Physique du Globe de Paris. SOI provided the R/V *Falkor* for the experiment and EOS funded the renting of the seismic equipment. The French participation was funded by IPG Paris and INSU-CNRS. This study is also supported by Guangdong Province Introduced Innovative R&D Team of Geological Processes and Natural Disasters around the South China Sea (2016ZT06N331), the National Key Research and Development Program of China (2017YFC1500101) and National Natural Science Foundation of China (41976197). We would like to thank the Captain and the team of R/V *Falkor* for their help and support during the experiment. We thank B. Benaïche, E. Duyck and C. Deplus for discussions and help with backscatter data processing. We thank G. Lamarche for comments on an earlier version of the manuscript, as well as two anonymous reviewers and editor J.P. Avouac for their constructive comments on this version, and E. Hill for discussions. Raw and processed EM302 (multibeam echo-sounder) data are available at http://www.marine-geo.org/tools/new_search/index.php?&output_info_all=on&entry_id=FK150523. Seismic reflection data are available upon request. SRTM and GEBCO data were accessed in October 2014 here: <http://www2.jpl.nasa.gov/srtm> and <http://www.gebco.net>. This is Earth Observatory of Singapore publication number 287.

Appendix A. Supplementary material

Supplementary material related to this article can be found online at <https://doi.org/10.1016/j.epsl.2020.116197>.

References

- Abercrombie, R.E., Antolik, M., Felzer, K., Ekström, G., 2001. The 1994 Java tsunami earthquake: slip over a subducting seamount. *J. Geophys. Res.* 106, 6595–6607.
- Almeida, R., Lindsey, E.O., Bradley, K., Hubbard, J., Mallick, R., Hill, E.M., 2018. Can the updip limit of frictional locking on megathrusts be detected geodetically? Quantifying the effect of stress shadows on near-trench coupling. *Geophys. Res. Lett.* 45 (10), 4754–4763.
- Ammon, C.J., Kanamori, H., Lay, T., Velasco, A.A., 2006. The 17 July 2006 Java tsunami earthquake. *Geophys. Res. Lett.* 33, L24308.
- Barnes, P.M., Lamarche, G., Bialas, J., Henrys, S., Pecher, I., Netzeband, G.L., Greinert, J., Mountjoy, J.J., Pedley, K., Crutchley, G., 2010. Tectonic and geological framework for gas hydrates and cold seeps on the Hikurangi subduction margin, New Zealand. *Mar. Geol.* 272 (1–4), 26–48.
- Bell, R., Holden, C., Power, W., Wang, X., Downes, G., 2014. Hikurangi margin tsunami earthquake generated by slow seismic rupture over a subducted seamount. *Earth Planet. Sci. Lett.* 397, 1–9.
- Bilek, S.L., Engdahl, E.R., DeShon, H.R., Hariri, M.E., 2011. The 25 October 2010 Sumatra tsunami earthquake: slip in a slow patch. *Geophys. Res. Lett.* 38, L1406.
- Bilek, S.L., Lay, T., 2002. Tsunami earthquakes possibly widespread manifestations of frictional conditional stability. *Geophys. Res. Lett.* 29, 1673.
- Bradley, K., Qin, Y., Carton, H., Hananto, N., Villanueva-Robles, F., Leclerc, F., Shengji, W., Tapponnier, P., Sieh, K., Singh, S., 2019. Stratigraphic control of frontal décollement level and structural vergence, and implications for tsunamigenic earthquake hazard in Sumatra, Indonesia. *Geochem. Geophys. Geosyst.*
- Chlieh, M., Avouac, J.-P., Sieh, K., Natawidjaja, D.H., Galetzka, J., 2008. Heterogeneous coupling of the Sumatran megathrust constrained by geodetic and paleogeodetic measurements. *J. Geophys. Res.* 113, B5.
- Costa, E., Vendeville, B.C., 2002. Experimental insights on the geometry and kinematics of fold-and-thrust belts above weak, viscous evaporitic décollement. *J. Struct. Geol.* 24, 1729–1739.
- Cummins, P.R., Kaneda, Y., 2000. Possible splay fault slip during the 1946 Nankai earthquake. *Geophys. Res. Lett.* 27, 2725–2728.
- Davis, D.M., Engelder, T., 1985. The role of salt in fold-and-thrust belts. *Tectonophysics* 119, 67–88.
- El Hariri, M., Bilek, S.L., DeShon, H.R., Engdahl, E.R., Bisrat, S., 2013. Along-strike variability of rupture duration in subduction zone earthquakes. *J. Geophys. Res.* 118, 646–664.
- Feng, L., Barbot, S., Hill, E.M., Hermawan, I., Banerjee, P., Natawidjaja, D.H., 2016. Footprints of past earthquakes revealed in the afterslip of the 2010 M_w 7.8 Mentawai tsunami earthquake. *Geophys. Res. Lett.* 43 (18), 9518–9526.
- Franke, D., Schnabel, M., Ladage, S., Tappin, D.R., Neben, S., Djajidihardja, Y.S., Müller, C., Kopp, H., Gaedicke, C., 2008. The great Sumatra–Andaman earthquakes—imaging the boundary between the ruptures of the great 2004 and 2005 earthquakes. *Earth Planet. Sci. Lett.* 269 (1–2), 118–130.
- Fujiwara, T., Kodaira, S., No, T., Kaiho, Y., Takahashi, N., Kaneda, Y., 2011. The 2011 Tohoku-Oki earthquake: displacement reaching the trench axis. *Science* 334 (6060), 1240.
- Graveleau, F., Malavieille, J., Dominguez, S., 2012. Experimental modelling of orogenic wedges: a review. *Tectonophysics* 538–540, 1–66.
- Hill, E.M., Borrero, J.C., Huang, Z., Qiu, Q., Banerjee, P., Natawidjaja, D.H., et al., 2012. The 2010 M_w 7.8 Mentawai earthquake: very shallow source of a rare tsunami earthquake determined from tsunami field survey and near-field GPS data. *J. Geophys. Res., Solid Earth* 117 (B6).
- Hubbard, J., Barbot, S., Hill, E., Tapponnier, P., 2015. Coseismic slip on shallow décollement megathrusts: implications for seismic and tsunami hazard. *Earth-Sci. Rev.* 141, 45–55.
- Hubert-Ferrari, A., Suppe, J., Gonzalez-Mieres, R., Wang, X., 2007. Mechanisms of active folding of the landscape (southern Tian Shan, China). *J. Geophys. Res., Solid Earth* 112 (B3).
- Ide, S., Baltay, A., Beroza, G., 2011. Shallow dynamic overshoot and energetic deep rupture in the 2011 M_w 9.0 Tohoku-Oki earthquake. *Science* 302, 1426–1429.
- Kanamori, H., 1972. Mechanism of tsunami earthquakes. *Phys. Earth Planet. Inter.* 6, 346–359.
- Kanamori, H., Rivera, L., Lee, W.H.K., 2010. Historical seismograms for unraveling a mysterious earthquake: the 1907 Sumatra earthquake. *Geophys. J. Int.* 183, 358–374.
- Kanamori, H., Kikuchi, M., 1993. The 1992 Nicaragua earthquake: a slow tsunami earthquake associated with subducted sediments. *Nature* 361, 714–716.
- Kodaira, S., No, T., Nakamura, Y., Fujiwara, T., Kaiho, Y., Miura, S., Takahashi, N., Kaneda, Y., Taira, A., 2012. Coseismic fault rupture at the trench axis during the 2011 Tohoku-oki earthquake. *Nat. Geosci.* 5 (9), 646.
- Konca, A.O., Avouac, J.P., Sladen, A., Meltzner, A.J., Sieh, K., Fang, P., Li, Z., Galetzka, J., Genrich, J., Chlieh, M., Natawidjaja, D.H., 2008. Partial rupture of a locked patch

- of the Sumatra megathrust during the 2007 earthquake sequence. *Nature* 456 (7222), 631.
- Konstantinovskaya, E., Malavieille, J., 2011. Thrust wedges with décollement levels and syntectonic erosion: a view from analog models. *Tectonophysics* 502 (3–4), 336–350.
- Kuncoro, A.K., Cubas, N., Singh, S.C., Etchebes, M., Tapponnier, P., 2015. Tsunamiogenic potential due to frontal rupturing in the Sumatra locked zone. *Earth Planet. Sci. Lett.* 432, 311–322.
- Lay, T., Ammon, C.J., Kanamori, H., Yamazaki, Y., Cheung, K.F., Hutko, A.R., 2011. The 25 October 2010 Mentawai tsunami earthquake (Mw 7.8) and the tsunami hazard presented by shallow megathrust ruptures. *Geophys. Res. Lett.* 38 (6).
- Lay, T., Kanamori, H., Ammon, C.J., Koper, K.D., Hutko, A.R., Ye, L., Yue, H., Rushing, T.M., 2012. Depth-varying rupture properties of subduction zone megathrust faults. *J. Geophys. Res., Solid Earth* 117 (B4).
- Li, L., Switzer, A.D., Wang, Y., Weiss, R., Qiu, Q., Chan, C.H., Tapponnier, P., 2015. What caused the mysterious eighteenth century tsunami that struck the south-west Taiwan coast? *Geophys. Res. Lett.* 42 (20), 8498–8506.
- Lindsey, J.P., 1989. The Fresnel zone and its interpretive significance. *Lead. Edge* 10, 33–39.
- Malavieille, J., Konstantinovskaya, E., 2010. Impact of surface processes on the growth of orogenic wedges: insights from analog models and case studies. *Geotectonics* 44, 541–558.
- McKenzie, D., Jackson, J., 2012. Tsunami earthquake generation by the release of gravitational potential energy. *Earth Planet. Sci. Lett.* 345, 1–8.
- McClay, K.R., 1992. In: McClay, K.R. (Ed.), *Thrust Tectonics*. Chapman & Hall, London, United Kingdom, pp. 419–433.
- Moore, G.F., Park, J.O., Bangs, N.L., Gulick, S.P., Tobin, H.J., Nakamura, Y., Sato, S., Tsuji, T., Yoro, T., Tanaka, H., Uraki, S., 2009. Structural and seismic stratigraphic framework of the NanTroSEIZE stage 1 transect. In: *Proc. IODP|Volume*, vol. 314, p. 2, No. 315/316.
- Moore, G.F., Saffer, D., Studer, M., Costa Pisani, P., 2011. Structural restoration of thrusts at the toe of the Nankai Trough accretionary prism off Shikoku Island, Japan: implications for dewatering processes. *Geochem. Geophys. Geosyst.* 12, Q0AD12.
- Newman, A.V., Hayes, G., Wei, Y., Convers, J., 2011. The 25 October 2010 Mentawai tsunami earthquake, from real-time discriminants, finite-fault rupture, and tsunami excitation. *Geophys. Res. Lett.* 38, L05302.
- Okada, Y., 1985. Surface deformation due to shear and tensile faults in a half-space. *Bull. Seismol. Soc. Am.* 75, 1135–1154.
- Okal, E.A., Newman, A.V., 2001. Tsunami earthquakes: the quest for a regional signal. *Phys. Earth Planet. Inter.* 124 (1–2), 45–70.
- Pelayo, A.M., Wiens, D.A., 1992. Tsunami earthquakes: slow thrust-faulting events in the accretionary wedge. *J. Geophys. Res.* 97, 15321–15337.
- Polet, J., Kanamori, H., 2000. Shallow subduction zone earthquakes and their tsunamigenic potential. *Geophys. J. Int.* 142, 684–702.
- Qin, Y., Singh, S.C., 2018. Insight into frontal seismogenic zone in the Mentawai locked region from seismic full waveform inversion of Ultralong Offset Streamer Data. *Geochem. Geophys. Geosyst.* 19 (11), 4342–4365.
- Saito, T., Furumura, T., 2009. Three-dimensional tsunami generation simulation due to sea-bottom deformation and its interpretation based on the linear theory. *Geophys. J. Int.* 178 (2), 877–888.
- Satake, K., Nishimura, Y., Putra, P.S., Gusman, A.R., Sunendar, H., Fujii, Y., Tanioka, Y., Latief, H., Yulianto, E., 2013. Tsunami source of the 2010 Mentawai, Indonesia earthquake inferred from tsunami field survey and waveform modeling. *Pure Appl. Geophys.* 170 (9–10), 1567–1582.
- Satake, K., Tanioka, Y., 1999. Sources of tsunami and tsunamigenic earthquakes in subduction zones. *Pure Appl. Geophys.* 154, 467–483.
- Shi, F., Kirby, J.T., Harris, J.C., Geiman, J.D., Grilli, S.T., 2012. A high-order adaptive time-stepping TVD solver for Boussinesq modeling of breaking waves and coastal inundation. *Ocean Model.* 43–44, 36–51.
- Sieh, K., Natawidjaja, D.H., Meltzner, A.J., Shen, C.C., Cheng, H., Li, K.S., Suwargadi, B.W., Galetzka, J., Philibosian, B., Edwards, R.L., 2008. Earthquake supercycles inferred from sea-level changes recorded in the corals of West Sumatra. *Science* 322 (5908), 1674–1678.
- Singh, S.C., Carton, H., Tapponnier, P., Hananto, N.D., Chauhan, A.P., Hartoyo, D., Bayly, M., Moeljopranoto, S., Bunting, T., Christie, P., Lubis, H., 2008. Seismic evidence for broken oceanic crust in the 2004 Sumatra earthquake epicentral region. *Nat. Geosci.* 1 (11), 777.
- Singh, S.C., Midenet, S., Djajadihardja, Y., 2009. Seismic survey of the locked and unlocked Sumatra subduction zone. *Eos* 90, 471–478.
- Singh, S.C., Hananto, N., Mukti, M., Permana, H., Djajadihardja, Y., Harjono, H., 2011. Seismic images of the megathrust rupture during the 25th October 2010 Pagai earthquake, SW Sumatra: frontal rupture and large tsunami. *Geophys. Res. Lett.* 38 (16).
- Tanioka, Y., Satake, K., 1996. Tsunami generation by horizontal displacement of ocean bottom. *Geophys. Res. Lett.* 23, 861–864.
- Tanioka, Y., Seno, T., 2001. Sediment effect on tsunami generation of the 1896 Sanriku tsunami earthquake. *Geophys. Res. Lett.* 28, 3389–3392.
- Tappin, D.R., Grilli, S.T., Harris, J.C., Geller, R.J., Masterlark, T., Kirby, J.T., Shi, F., Ma, G., Thingbaijam, K.K.S., Mai, P.M., 2014. Did a submarine landslide contribute to the 2011 Tohoku tsunami? *Mar. Geol.* 357, 344–361.
- Tehraniad, B., Shi, F., Kirby, J., Harris, J.C., Grilli, S., 2011. Tsunami Benchmark Results for Fully Nonlinear Boussinesq Wave Model FUNWAVE-TVD, Version 1.0 Rep. Center for Applied Coastal Research, University of Delaware, Newark.
- Tsang, L.L., Hill, E.M., Barbot, S., Qiu, Q., Feng, L., Hermawan, I., Banerjee, P., Natawidjaja, D.H., 2016. Afterslip following the 2007 M_w 8.4 Bengkulu earthquake in Sumatra loaded the 2010 M_w 7.8 Mentawai tsunami earthquake rupture zone. *J. Geophys. Res., Solid Earth* 121 (12), 9034–9049.
- von Huene, R., Miller, J.J., Weinrebe, W., 2012. Subducting plate geology in three great earthquake ruptures of the western Alaska margin, Kodiak to Unimak. *Geosphere* 8, 628–644.
- Vannucchi, P., Spagnuolo, E., Aretusini, S., Di Toro, G., Ujiie, K., Tsutsumi, A., Nielsen, S., 2017. Past seismic slip-to-the-trench recorded in Central America megathrust. *Nat. Geosci.* 10 (12), 935.
- Wang, R., Martin, F.L., Roth, F., 2003. Computation of deformation induced by earthquakes in a multi-layered elastic crust: FORTRAN programs EDGRN/EDCMP. *Comput. Geosci.* 29, 195–207.
- Yelisetti, S., Spence, G.D., Scherwath, M., Riedel, M., Klaeschen, D., 2017. Dual-vergence structure from multiple migration of widely spaced OBSs. *Tectonophysics* 718, 45–60.
- Yue, H., Lay, T., Rivera, L., Bai, Y., Yamazaki, Y., Cheung, K.F., Hill, E.M., Sieh, K., Kongko, W., Muhari, A., 2014. Rupture process of the 2010 M_w 7.8 Mentawai tsunami earthquake from joint inversion of near-field hr-GPS and teleseismic body wave recordings constrained by tsunami observations. *J. Geophys. Res., Solid Earth* 119 (7), 5574–5593.